Partition Speeds Up Learning Implicit Neural Representations Based on Exponential-Increase Hypothesis

Ke Liu[1], Feng Liu[2], Haishuai Wang[1*], Ning Ma[1], Jiajun Bu[1], Bo Han[3]

[1] Zhejiang Provincial Key Laboratory of Service Robot,
College of Computer Science, Zhejiang University, Hangzhou, China
[2]School of Computing and Information Systems, The University of Melbourne, Australia
[3]Department of Computer Science, Hong Kong Baptist University, Hong Kong SAR, China

{keliu99, haishuai.wang, ma_ning, bjj}@zju.edu.cn,
fengliu.ml@gmail.com, bhanml@comp.hkbu.edu.hk

Abstract

Implicit neural representations (INRs) aim to learn a continuous function (i.e., a neural network) to represent an image, where the input and output of the function are pixel coordinates and RGB/Gray values, respectively. However, images tend to consist of many objects whose colors are not perfectly consistent, resulting in the challenge that image is actually a discontinuous piecewise function and cannot be well estimated by a continuous function. In this paper, we empirically investigate that if a neural network is enforced to fit a discontinuous piecewise function to reach a fixed small error, the time costs will increase exponentially with respect to the boundaries in the spatial domain of the target signal. We name this phenomenon the exponential-increase hypothesis. Under the exponential-increase hypothesis, learning INRs for images with many objects will converge very slowly. To address this issue, we first prove that partitioning a complex signal into several sub-regions and utilizing piecewise INRs to fit that signal can significantly speed up the convergence. Based on this fact, we introduce a simple partition mechanism to boost the performance of two INR methods for image reconstruction: one for learning INRs, and the other for learning-to-learn INRs. In both cases, we partition an image into different sub-regions and dedicate smaller networks for each part. In addition, we further propose two partition rules based on regular grids and semantic segmentation maps, respectively. Extensive experiments validate the effectiveness of the proposed partitioning methods in terms of learning INR for a single image (ordinary learning framework) and the learning-to-learn framework. Code is released here.

*Corresponding author: Haishuai Wang (haishuai.wang@zju.edu.cn)

1. Introduction

Recently, an innovative model for data/signal representation called implicit neural representations (INRs) has aroused researchers' great attention, due to their remarkable visual performance in computer vision tasks, including image generation [29, 9, 31, 4] and novel views synthesis [12]. To fit such an *implicit neural representation* for a 2D image, we usually learn a continuous function formalized by a neural network, which takes space coordinates $x \in \mathbb{R}^2$ as input and outputs the color values at the queried coordinate ($y \in \mathbb{R}^3$ if RGB and $y \in \mathbb{R}$ if gray).

However, in-the-wild images are actually *discontinuous piecewise functions*. They consist of discrete objects with not perfectly consistent colors (as shown in Figure 1(a)). Large gradients exist on the boundaries between two discontinuous parts, preventing the neural network from converging to a small error when fitting images. To study the above issue, related research called "spectral bias" [19, 34] has proved that neural networks prioritize learning the low-frequency components. Yet, they only describe this phenomenon from the view of the implicit frequency domain and do not propose a quantitative relation between the convergence rate and the attribute of the target signal.

In this paper, we first re-examine the above phenomenon from the explicit spatial domain and empirically investigate a quantitative relation: the time complexity of fitting a discontinuous piecewise function with a neural network would increase exponentially with respect to the number of boundaries. For example, in Figure 1(b) and 1(c), we use SIREN MLPs [29] to fit 1D synthetic signals and 2D synthetic signals where N boundaries exist in their spatial domain. We then explore the relation between the required convergence step n and the number of boundaries N, and find that the relation curves align with the exponential function. We

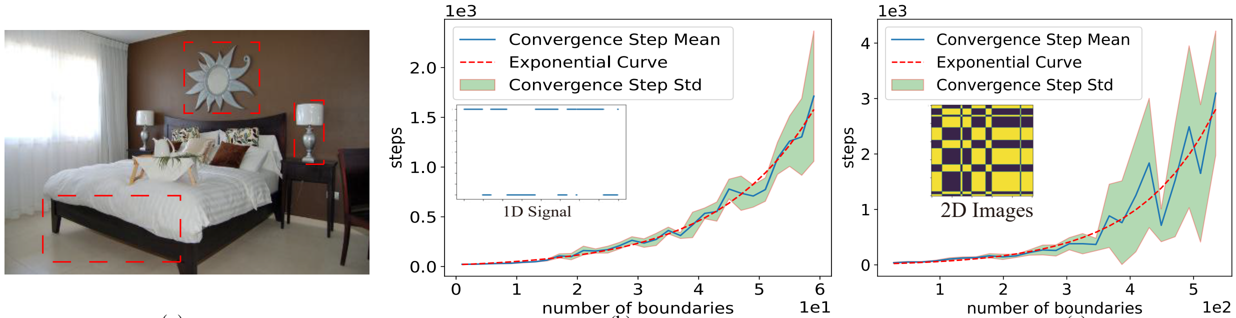

(a) (b) (c)

Figure 1. (a) Discontinuous parts exist obviously in regions with red boxes, which motivates us to use piecewise functions to represent the complex signals. (b) & (c) We dedicate a single neural network to fit the 1D and 2D synthetic signals with N boundaries. The results show that the relation between the convergence step n and the number of boundaries N align with the exponential function $n \propto O(p^N)$, where $p = 1.0656$ for 1D synthetic signals and $p = 1.00815$ for 2D synthetic signals. The detailed experiment is presented in Appendix A.

call this phenomenon the *exponential-increase* hypothesis. Under this hypothesis, the optimization process of fitting a high-resolution in-the-wild image with a single continuous INR will converge at a *slow rate*.

Based on the exponential-increase hypothesis, we mathematically prove that partitioning images into several parts and learning INRs within each part can reduce the exponential complexity to linear complexity and significantly decrease the convergence time. In light of this fact, we propose partition-based INR methods and utilize partition in two INR frameworks: one for learning INRs, and the other for learning-to-learn INRs. Specifically, in both frameworks, we partition an image into different sub-regions based on particular rules and dedicate smaller networks for each sub-region. We also propose two partition rules: one is based on regular grids, and the other is based on semantic segmentation maps. Both of them can speed up the convergence of learning INRs as well as learning-to-learn INRs. In summary, the contributions of this work are as follows.

- From the view of spatial domains, we investigate the exponential relation between the network convergence rate and the number of boundaries in the target signals, namely the exponential-increase hypothesis.
- Based on the exponential-increase hypothesis, we mathematically prove that partition reduces the exponential complexity of fitting all boundaries to the linear complexity of fitting separate regions.
- We propose partition-based learning and learning-to-learn INRs frameworks for image reconstruction task. We also propose two partition rules that are based on regular grids or semantic segmentation maps.
- Extensive experiments on image reconstruction show that (i) partition boosts learning INRs framework to faster convergence, (ii) partition boosts learning-to-learn INRs framework to better reconstruction performance with fixed optimization steps.

2. Related Work

Implicit Neural Representations. Implicit Neural Representations (INRs) [39] are emerging topics of interest in the artificial intelligence community. By mapping a coordinate x to a quantity with a neural network (e.g., MLP), these continuous representations have shown great potential in 3D scene reconstruction [6, 8, 16, 11], digital humans tasks [42, 25, 26], 2D images generation [18, 29, 31, 46], 3D shape and appearance generation [7, 27, 14, 12], video representation [1], physics-informed problems [20, 17] and so on. A lot of works have been conducted on different aspects of INRs, such as the prior learning and conditioning [30, 35, 37], the computation and memory efficiency [10], the expression capacity [21, 44], the edit ability [30] and the generalization across different samples [28, 33].

Partition Techniques. When scaling up to signals with large domains, INRs always fail due to the high nonlinearity of mapping function [23] and heavy time consumption. Thus, partition are extensively employed, e.g. Voronoi spatial decomposition by DeRF [21], distillation for training thousands of MLPs by KiloNeRF [22], multiscale block-coordinate decomposition by ACRON [9], scalable large-scale NeRF [32, 36]. Although these works have a good effect on representing large-scale images or scenes, they seldom discuss why partition improves the training efficiency of learning single INR and do not discuss the effect of partition on the learning-to-learn INRs framework.

Neural Network Spectral Bias. Spectral bias [19, 40], or frequency principle [41, 24], is a phenomenon that neural networks prioritize learning the low-frequency parts of signals. Lots of works have been presented to enable an MLP to fit high-frequency functions, e.g. Fourier feature mapping by Tancik *et al*. [34] and periodic activation functions by Sitzmann *et al*. [29]. In this paper, we re-examine the spectral bias and propose the exponential-increase hypothesis from the spatial domain, which is an explicit and

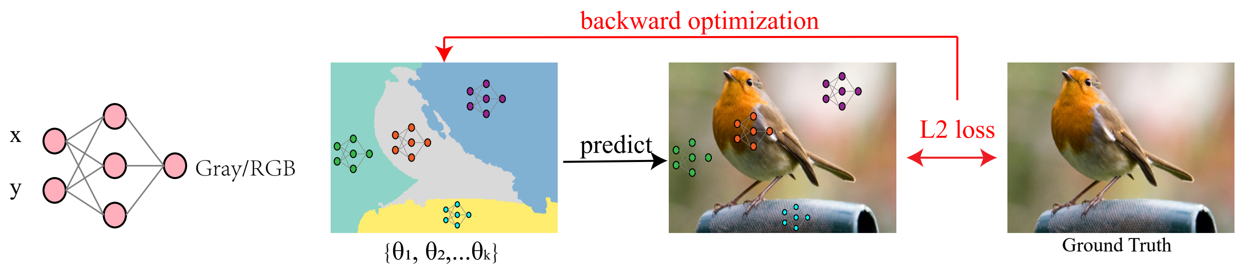

(a) MLP for INRs

(b) Framework for partition-based INR training paradigm

Figure 2. (a) MLP architecture for image INR. The inputs are the coordinates $(x, y) \in \mathbb{R}^2$ and the outputs are Gray/ RGB values. (b) Framework for partition-based Learning INRs. We dedicate different MLPs to fit different parts of the image.

quantitative description of the relation between the network convergence rate and the properties of the target signals.

Learning-to-learn INRs. Meta-learning is applied to train a meta-learner that can quickly adapt to new tasks with few training examples. MetaSDF [28] first introduced MAML [5] to learn excellent INR priors over the respective function space, leading to faster fine-tuning and better geometry reconstruction. Tancik *et al*. [33] re-produced such findings with Reptile [13] on a wider variety of signal types. Yuce *et al*. [44] presented a theoretical analysis of meta-learning INRs from the view of dictionary learning. Based on these works, we show that partition in INR meta-learning framework can modulate the spectral bias within each partition part and improve the effect of learning-to-learn INRs.

3. Partition for learning and learning-to-learn Implicit Neural Representations

Motivations Considering a field $\mathbf{q}$ and coordinate $\mathbf{x}$, INR learns a function Φ with parameters Θ to fit it, which is denoted as $\mathbf{q} = \Phi(\mathbf{x}; \Theta)$. SIREN [29] shows that MLPs with ReLU activation fail to represent the derivatives of the target signal. So they propose periodic activation functions to represent complex signals and their derivatives. However, even though SIREN is able to represent complex signals, a lot of optimization steps are required due to the fact that too many boundaries with large gradients exist in the spatial domain of the complex signal. We argue that the events of successfully representing each boundary with a large gradient by the neural network parameters Θ are independent with each other. Then we establish the following hypothesis:

Hypothesis 1. *Denote the complexity that one boundary with large derivatives is represented by Θ as p, then the complexity that all boundaries are represented by Θ is $O(p^N)$, where N is the number of boundaries with large derivatives within the spatial domain.*

We name this hypothesis the exponential-increase hypothesis. Experiments to demonstrate this hypothesis are shown in Appendix A. To mitigate the issue caused by this hypothesis, we deliver partition to reduce the exponential complexity of fitting all boundaries to the linear complexity of fitting several regions. Specifically, we divide the whole domain into smaller domains and use independent MLPs to fit a piecewise function to represent the whole function.

Formally, if the whole domain is divided into k sub-domains, the number of boundaries falling in each sub-domain are $\{N_1, N_2, ..., N_k\}$, where $N = \sum_{i=1}^{k} N_i$. We argue that the optimizations for all MLPs are parallel. If we dedicate neural networks with full capacity to fit each sub-domain, we can assume the complexity of fitting one boundary is still p, then the total complexity of parallelly fitting all sub-domains with separate neural networks is

$$p^{N_1} + p^{N_2} + ... + p^{N_k} = \sum_{i=1}^{k} p^{N_i}. \tag{1}$$

Then we can establish the following proposition:

Proposition 1. *In case of $k \geq 3$, the complexity of dedicating neural networks with full capacity for each sub-domain is less than the complexity of representing the whole domain with a single neural network, i.e. $\sum_{i=1}^{k} p^{N_i} < p^N$.*

Proof. Defining $\hat{N} = \max(N_1, N_2, ..., N_k)$, we have:

$$\frac{\sum_{i=1}^{k} p^{N_i}}{p^{\hat{N}}} = \sum_{i=1}^{k} \frac{p^{N_i}}{p^{\hat{N}}} \leq \sum_{i=1}^{k} 1 = k. \tag{2}$$

Empirically, we should optimize each neural network at least several times, so we have at least $p^{N_i} \geq 2$, then the following inequation holds:

$$\frac{p^N}{p^{\hat{N}}} = \frac{p^{(N_1+N_2+...+N_k)}}{p^{\hat{N}}} = \prod_{N_i \neq \hat{N}} p^{N_i} \geq 2^{k-1}. \tag{3}$$

In case of $k \geq 3$, we have $k < 2^{k-1}$ and $\sum_{i=1}^{k} p^{N_i} < p^N$. Proposition 1 is proved. □

Theoretically, with larger k, Proposition 1 can be generalized to the case of fitting each sub-domain with smaller neural networks, whose complexity of fitting one boundary is larger than p. We show the proof and the discussion of this case in Appendix B. Papers about the spectral bias of

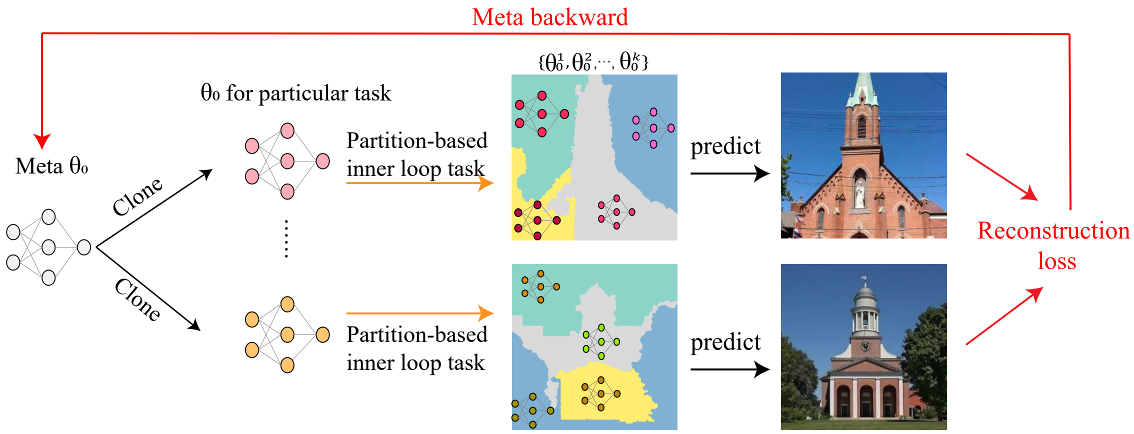

(a) Framework for partition-based learning-to-learn INRs

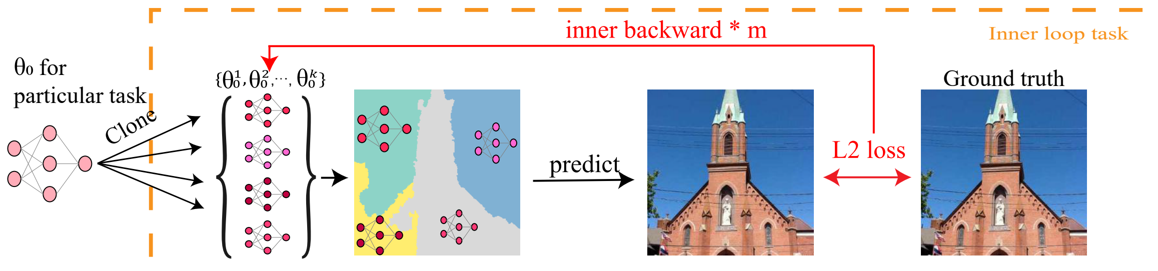

(b) Inner loop task for learning-to-learn INRs

Figure 3. (a) Framework for partition-based learning-to-learn INRs. A meta-learner is applied to sample tasks of learning INRs and learns an initialized weight that can quickly fine-tune to a new image. (b) Partition-based inner loop task. The initialized weights will be copied and then optimized for each head within its corresponding sub-domain. (Best view in color.)

INRs [19, 34, 44] show that INRs are hard to fit the signals with high-frequency components. In fact, the boundaries in the images are high-frequency components of signals and we show that partition helps to reduce the high-frequency components of the input signals in Appendix D.

By now, we have mathematically proved that partition can speed up the convergence of INRs by reducing the exponential complexity to linear complexity. And we will present how we practically utilize the partition methods in INRs in the following sections.

Partition for Learning INRs In this part, we show how we can apply partition to learning INRs for 2D images. The framework of the partition-based learning INR method is shown in Figure 2. We propose to model the INR of a given image I as a weighted sum of k neural networks (denoted as heads). Mathematically, this process can be expressed as

$$I(\mathbf{x}) = \sum_{n=1}^{k} \omega_\phi^n(\mathbf{x}) I_{\theta_n}(\mathbf{x}), \tag{4}$$

where n is the head index. $\omega_\phi^n(\mathbf{x}) : \mathbb{R}^2 \mapsto \{0,1\}$ is the mask for head n, and $\omega_\phi(\mathbf{x}) : (\omega_\phi^1(\mathbf{x}), \omega_\phi^2(\mathbf{x}), ..., \omega_\phi^k(\mathbf{x})) \in \{0,1\}^k$ is the mask for all heads and satisfies $\|\omega_\phi(\mathbf{x})\|_1 = 1$. This setting ensures that each coordinate in the image is only represented by one single head. When predicting an image, each coordinate is only required to be inputted into one single head. Therefore, both the time complexity and memory consumption of predicting the whole image with our partition-based models do not increase.

In practice, we explore two different partition rules for 2D images: one is based on regular grids and the other is based on semantic segmentation maps for 2D images. Detailed implementation is discussed in Section 4.

Partition for Learning to Learn INRs In [28, 33], they have shown that meta-learning algorithms can provide excellent initial weight parameters for learning INRs, which leads to faster convergence and better generalization. In this part, we show that our partition methods can be integrated into the meta-learning algorithm for INRs, and lead to better generalization and a more flexible inference process than the original meta-learning algorithm for INRs.

Considering a dataset including observations of signals T from a particular distribution $\mathcal{T}$ and a fixed number of optimization steps m, the meta-learning algorithms for INRs seek to find an initial weight θ_0^* that will result in the lowest possible final loss $L(\theta_m)$ if optimizing a network f_θ for m steps to represent a new signal from $\mathcal{T}$:

$$\theta_0^* = \arg\min_{\theta_0} E_{T\sim\mathcal{T}}\left[L\left(\theta_m\left(\theta_0, T\right)\right)\right]. \tag{5}$$

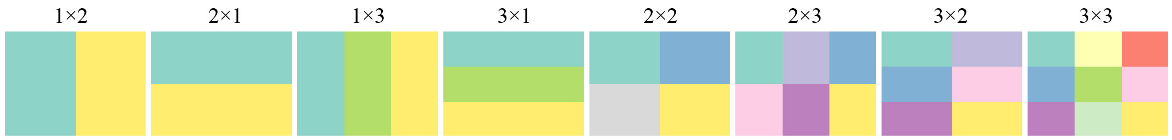

(a) Examples for partition based on regular grid

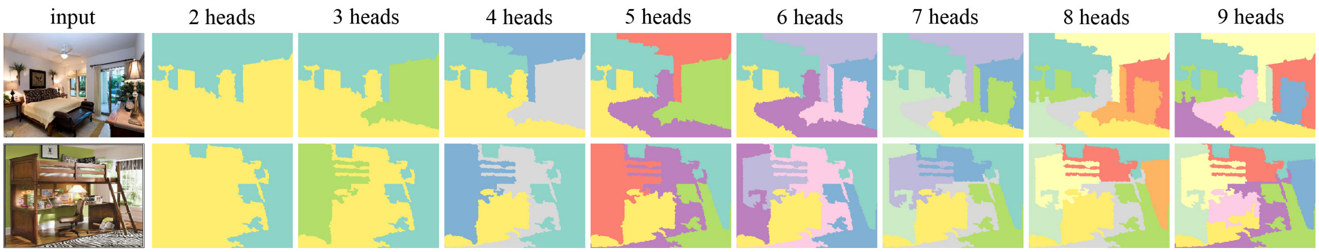

(b) Examples for partition based on segmentation

Figure 4. (a) Visualization of partition based on regular grids (PoG). (b) Visualization of partition based on HFS semantic segmentation maps (PoS). (Better view in color.)

Combining with partition techniques, we partition the whole input domain into k sub-domains with partition rule ω and seek to find an initial weight θ_0^* that serves as the initial weight of each head for each sub-domain. This will result in the lowest possible final total loss when optimizing a set of network $F = \{f_{\theta^1}, f_{\theta^2}, ..., f_{\theta^n},\}$, each of which will represent a part of the new signal from $\mathcal{T}$:

$$\theta_0^* = \arg\min_{\theta_0} E_{T\sim\mathcal{T}}\left[\sum_{n=1}^{k} L\left(\theta_m^n\left(\theta_0, T, \omega\right)\right)\right]. \tag{6}$$

We follow MAML [5] to learn an initial weight that can serve as a good starting point for gradient descent for all heads. Specifically, given a task T and the number of optimization steps m, our partition-based learning-to-learn INRs framework treats these task-specific optimization steps as inner loops, and wraps an outer loop to sample different signals T_j from $\mathcal{T}$. We generate their corresponding partition rules ω_j to learn the initial weight θ_0^*. Denote the meta-learning rate as β and the parameters of head k at i inner loop step and j outer loop step as $(\theta_i^k)_j$, then the updated rule of the parameters is defined as follows:

$$(\theta_0)_{j+1} = (\theta_0)_j - \beta\nabla_\theta \sum_{n=1}^{k} L\left(\theta_m^n\left((\theta_0)_j, T_j, \omega_j\right)\right). \tag{7}$$

The experiments are conducted in 2D image reconstruction, and direct point-wise observations of the signal T are available. Therefore, we can supervise F with gradient descent using simple L2 loss:

$$L(\theta) = \sum_i \left\|F\left(\mathbf{x}_i\right) - T\left(\mathbf{x}_i\right)\right\|_2^2. \tag{8}$$

So far, we have presented our partition-based learning INRs method as well as the partition-based learning-to-learn INRs method. The architectures of these two methods are presented in Figure 2 and 3 respectively.

4. Implementation

In this section, we introduce two partition rules that both work well under our frameworks. One is based on regular grids (PoG for short) and the other is based on semantic segmentation maps (PoS for short).

Partition based on regular grids. A simple but efficient partition rule is using regular grids to decompose the whole input domain. This method is widely used in image processing tasks based on ViT [3], while [21, 22] have discussed the effect of regular grids decomposition in neural radiance fields tasks. Specifically, for 2D images, we subdivide the input domain into uniform grids of resolution $\mathbf{r} = (r_x, r_y)$, and utilize an independent neural network to fit the content within each grid. Therefore the mapping function m from the pixel position $\mathbf{x}$ to its corresponding neural network index is defined as:

$$m(\mathbf{x}) = \left\lfloor \frac{\mathbf{x}}{\mathbf{r}} \right\rfloor. \tag{9}$$

Partition based on Semantic Segmentation Maps. We also seek a more flexible and reasonable partition rule, due to the fact that the real images contain non-homogeneous structures and the regular grid partition may violate the continuity of the images. Considering that an in-the-wild image always consists of several parts, it is reasonable to define a sub-domain as the region in which all pixels belong to the same part. Therefore, we seek a partition rule based on image semantic segmentation maps. It is clear that partitioning images based on their semantic segmentation maps helps to reduce the boundaries (or high-frequency components) within each partition part.

Specifically, we start with a hierarchical feature selection (HFS) [2] algorithm, which is a rapid image segmentation system and reports over-segmentation results. The over-segmentation results usually assign the regions that are

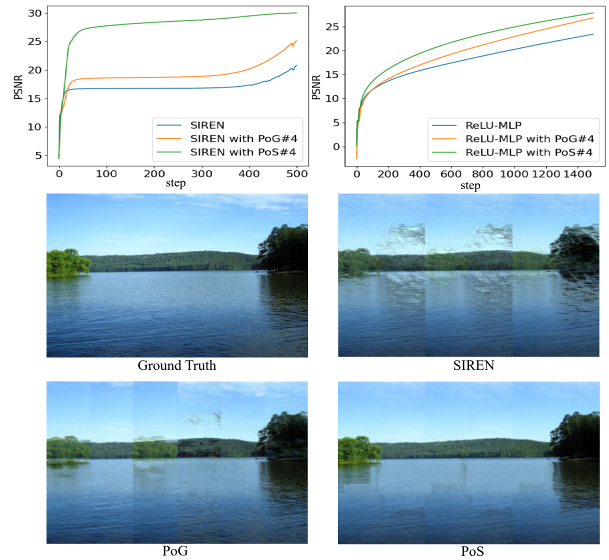

Figure 5. The first row presents PSNR vs. step curves for fitting the ground truth image with SIREN-based models and ReLU-MLP-based models (4 heads). The second and third rows present the visual results of optimizing siren-based models for 500 steps. Results from models with partition contain much fewer artifacts with the same optimization steps.

not connected with the same labels and the number of regions is always too large. Thus, we apply the connected-components algorithm on the initial segmentation results to re-label those unconnected parts. And we finally apply a greedy region-merging algorithm to obtain segmentation results with a particular number of regions.

The performance of PoG and PoS methods are demonstrated in Figure 4 while we present the formalization of the PoS algorithm in Appendix C.

5. Experiments

In this part, we will first compare the convergence speed of learning the INR for a single in-the-wild image with two modern MLP architectures under the condition of taking partition or not taking partition. We show that our partition methods achieve good performance on both two INR architectures. Then we choose SIREN [29] as our basic architecture and follow MetaSDF [28]'s setting to train meta models with or without partition.

5.1. Partition-based Learning INRs

Settings. We first choose a landscape image with dimension 380×254 (shown in Figure 5 ground truth) and try to learn an INR for this image. Two popular network architectures are chosen to evaluate our methods: one is SIREN with periodic activation functions [29] and the other is MLP with ReLU activation functions and positional embedding.

On top of these two baselines, our two partition rules are implemented. To fairly demonstrate the effect of our partition methods, we dedicate neural networks with the same architecture and hyper-parameters but smaller capacity to fit each sub-region, namely heads. We guarantee that the total capacity of all heads is close to the capacity of baselines. The detailed implementation of these two INR architectures as well as model parameter settings are presented in Appendix E. Following [29]'s implementation, we apply the Adam optimizer with a learning rate of $1e-4$. To make a comparison between the two partition methods, the number of partitioned regions is fixed to 4 (2×2 for PoG).

Results. We first present the PSNR curves with respect to optimization steps for applying partition methods on both two baselines, as shown in Figure 5 (the running time and memory consumption of partition-based models are the same or less than the baseline models, which will be discussed in Appendix G.). On both two baseline architectures, our two partition rules result in faster convergence, while partition based on semantic segmentation maps has better performance than partition based on regular grids. We can observe that for SIREN-based architecture, the model with PoS converges to a high PSNR with very limited steps (less than 100), while the original SIREN needs more than 500 steps to converge to the same PSNR value. For ReLU-MLP-based architecture, the required steps of three cases that the PSNR value reaches 20 are 957, 672, and 445 respectively, which indicates that our partition method based on regular grids (PoG) boosts to 50% speed-up while the partition method based on segmentation maps (PoS) results in 100% speed-up.

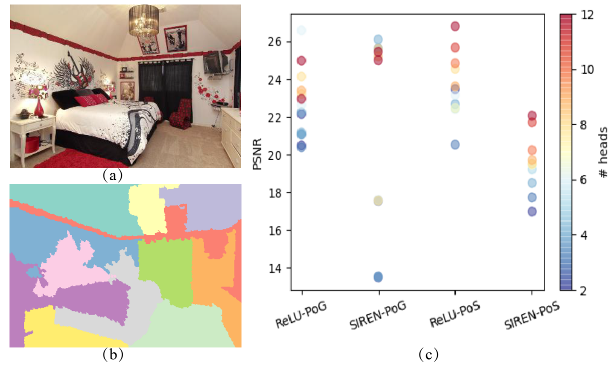

Figure 6. Typical results for applying models with different partitioned heads on images. (a) shows the original image and (b) shows its 12-part segmentation result. (c) presents the PSNR values of all models. The results indicate that models with more heads tend to achieve higher PSNR at fixed training steps.

Table 1. Mean PSNR values for LSUN test images. We optimize the SIREN-based models for 300 steps and ReLU-MLP-based models for 1000 steps. More results are in Appendix G

Methods	PSNRs↑	Methods	PSNRs↑
SIREN	21.211	ReLU-MLP	19.844
SIREN-PoG	23.864	ReLU-PoG	22.672
SIREN-PoS	**24.485**	ReLU-PoS	**22.863**

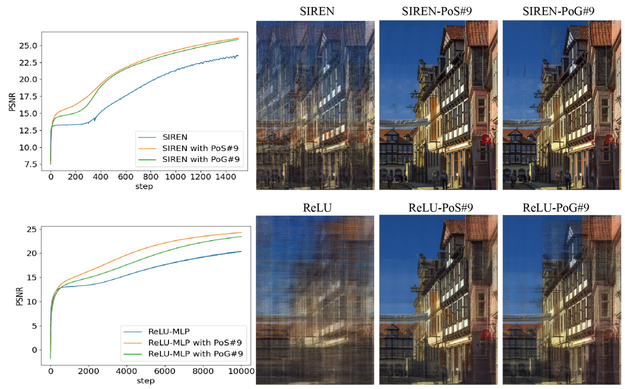

Figure 7. Training curves and intermediate results for example super-resolution image. The first row contains the experiments for SIREN-based models while the second row contains experiments for ReLU-MLP-based models. We present the intermediate results of optimizing SIREN-based models for 400 steps and optimizing ReLU-MLP-based models for 4000 steps.

Fewer artifacts for SIREN. As shown in Figure 5, SIREN [29] fails when fitting a large image and tends to generate periodic artifacts. This failure has been reported by [44] and is due to the imperfect frequency recovery. However, the results from our partition-based models generate fewer artifacts with the same optimization steps. This is because partition helps to reduce the high-frequency components that one single SIREN needs to represent, which partly alleviates the negative effect of SIREN.

Robustness. To prove the robustness of our partition methods, we also evaluate our methods on LSUN bedroom image test set [43], which contains 300 in-the-wild images. We explore the mean PSNR values with 300 optimization steps for SIREN-based models and 1000 optimization steps for ReLU-MLP-based models. The results are reported in Table 1. We can observe that both of our partition methods drive the models to a higher PSNR value with the same optimization steps.

More heads, faster convergence. We conduct experiments to find the optimal number of heads for both two architectures and two partition methods. A typical example is shown in Figure 6. With a different number of heads and two partition methods, we optimize SIREN-based models with 200 steps and ReLU-MLP-based models with 1200 steps. The results show that the models with more heads generally tend to converge to better results and achieve higher PSNR values at the fixed training step. Extensive experiments and discussions of models with different numbers of heads on more images are presented in Appendix F.

Scale to super-resolution images. Due to the previous conclusion, we can easily improve the INR optimization efficiency of super-resolution images by increasing the number of partition heads. A typical example of learning INRs for a super-resolution image with 700×1000 dimension is shown in Figure 7. By partitioning the whole image into 9 parts, we can significantly improve the reconstruction performance of both SIREN-based models and ReLU-MLP-based models. More experiments of learning INRs for super-resolution images are presented in Appendix G.

Table 2. Mean PSNR values performance for SIREN models with different training and fine-tuning methods. For short, we rewrite G as the PoG partition method and S as the PoS partition method. We mark a superscript G/S if we apply the corresponding method in the training stage and mark a subscript G/S if we apply the corresponding method in the fine-tuning stage.

Setting	PSNR ↑ 1 View	PSNR ↑ 3 View	Setting	PSNR ↑ 1 View	PSNR ↑ 3 View
SIREN	19.42	22.60	-	-	-
SIREN_G	19.64	22.95	SIREN_S	19.85	23.09
$\text{SIREN}_\text{G}^\text{G}$	19.77	**24.23**	$\text{SIREN}_\text{S}^\text{S}$	**20.00**	23.93
$\text{SIREN}_\text{G}^\text{S}$	19.93	23.89	$\text{SIREN}_\text{S}^\text{G}$	18.11	20.33

5.2. Partition-based Learning-to-learn INRs

Settings. To verify the effect of our partition-based learning-to-learn INRs framework, we follow MetaSDF [28] and apply our partition methods in the MAML framework to learn an initial weight that can quickly fine-tune to an unseen image. The outdoor church images from LSUN dataset [43] with the size of 256×256 are chosen for evaluating the method. The training set contains about 126k images and the test set includes 300 images. Following [28, 33], we choose SIREN as our basic model and set up the number of inner loop step N as 3, which means that our model sees each image only three times. We apply the per-parameter-per-step inner learning rate strategy with initial learning rate $\alpha = 1e - 5$. All of the meta-models are trained with an outer loop learning rate $\beta = 1e - 4$ and a batch size of 4.

Since our partition methods duplicate the initial weight for each head, we maintain one copy of per-parameter-per-step learning rates for a single head and share it with all heads. The SIREN model in our implementation contains 3 hidden layers and 128 hidden features, which is also the set-up for each head in our models with partition. As a result, the weights trained from the original SIREN and the weights trained from our partitioned-based models have the same keys. Thanks to these settings, in the inference phase we can fine-tune based on our partition methods with the initialized weights trained from the original SIREN.

Results. On top of baseline SIREN, We demonstrate the effect of our two partition methods both on the training phase and the inference phase. The mean PSNR values for 1 View and 3 View fine-tuning on 300 images based on models with different training and fine-tuning mechanisms are shown in Table 2. The results show that only fine-tuning based on our partition methods with the initialized weights trained from the original SIREN can lead to better performance than baseline, no matter whether we use

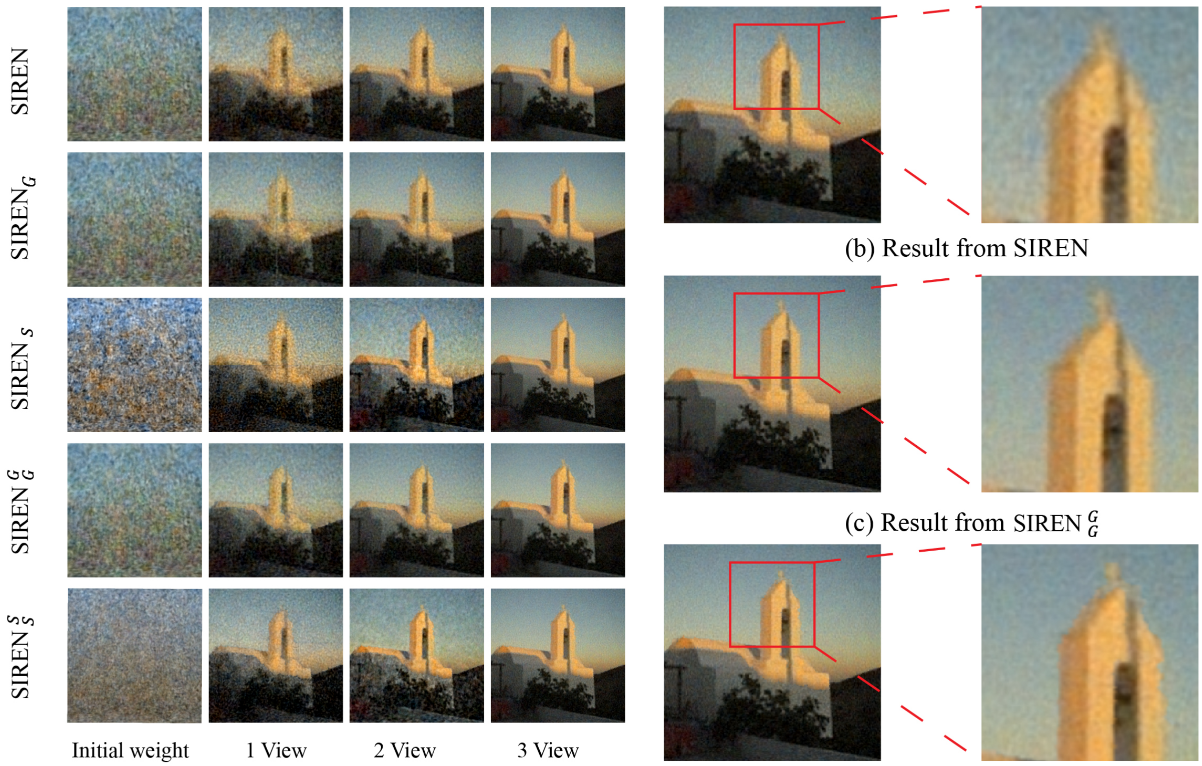

(a) Visual results for each step

(b) Result from SIREN

(c) Result from SIREN ^G_G

(d) Result from SIREN ^S_S

Figure 8. Visual results of models with different training and fine-tuning methods. The same abbreviation as in Table 2. The results from our partition-based models contain less noise and sharper edges than the SIREN model. (Better view in color.)

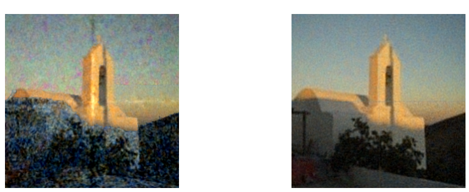

SIREN ^G_S SIREN ^S_G

Figure 9. Performance of fine-tuning with PoS on the PoG trained initialized weight, and its opposite case. The model trained with PoG but fine-tuned with PoS fails, while the model trained with PoS but fine-tuned with PoG achieves good performance. (Better view in color.)

PoG partition or PoS partition. And the experimental results also indicate that the model employing PoG partition during both training and inference phases exhibits the highest PSNR for 3 View fine-tuning, while the model utilizing PoS partition during both phases achieves the highest PSNR for 1 View fine-tuning. Therefore we prove that fine-tuning based on our partition methods with the initialized weight trained from the partition models has the best performance. For detailed description, a typical example is presented in Figure 8. The result shows that the images obtained from our partition methods contain less noise and sharper boundaries than the result from the baseline SIREN. More visual results and discussions are attached in Appendix H.

PoS partition as a more flexible choice. As shown in Figure 9, fine-tuning with the PoS method from the initialized weights trained with the PoG method leads to a poor result, while the opposite case still maintains good performance. This phenomenon meets our expectations because each head in the PoG method only learns to fit a regular region and fails to fit an irregular region when fine-tuning with the PoS method. On the contrary, the heads in the PoS method learn to fit regions with arbitrary shapes, including the regular grid. As a result, the PoS method can be considered more flexible than the PoG method.

6. Conclusion

In this paper, we investigate the dilemma of fitting a discontinuous signal via a continuous function (e.g., a neural network) and demonstrate that the time complexity to force a neural network to fit a discontinuous function is exponentially increasing with the number of high gradients in the input domain, which we call *exponential-increase* hypothesis. We consider the *exponential-increase* hypothesis as a quantitative description of spectral bias [19, 34, 44] from the spatial domain. We prove that partitioning the input domain into several sub-domains and dedicating smaller neural networks for each sub-domain help to alleviate this contradiction. Based on this observation, we propose two partition methods for learning and learning-to-learn INRs. We also present two partition rules: one is partitioning based on regular grids and the other is based on semantic segmentation maps. Our methods significantly speed up the convergence of learning INRs from scratch and also lead to better results for fine-tuning a new image at fixed steps for learning-to-learn INRs. Our findings in the paper can serve as theoretical support and inspire the follow-up work on learning more powerful INRs for in-the-wild scenes.

Acknowledgements

This work is supported by the National Natural Science Foundation of China (Grant Nos. 62202422 and 61972349), and the National Key Research and Development Program (Grant Nos. 2018YFB1403202, 2019YFF0302601, and 2020YFF0304905). BH is supported by NSFC Young Scientists Fund No. 62006202 and Guangdong Basic and Applied Basic Research Foundation No. 2022A1515011652.

References

[1] Hao Chen, Bo He, Hanyu Wang, Yixuan Ren, Ser Nam Lim, and Abhinav Shrivastava. Nerv: Neural representations for videos. *Advances in Neural Information Processing Systems*, 34:21557–21568, 2021. 2

[2] Ming-Ming Cheng, Yun Liu, Qibin Hou, Jiawang Bian, Philip Torr, Shi-Min Hu, and Zhuowen Tu. Hfs: Hierarchical feature selection for efficient image segmentation. In *European conference on computer vision*, pages 867–882. Springer, 2016. 5

[3] Alexey Dosovitskiy, Lucas Beyer, Alexander Kolesnikov, Dirk Weissenborn, Xiaohua Zhai, Thomas Unterthiner, Mostafa Dehghani, Matthias Minderer, Georg Heigold, Sylvain Gelly, et al. An image is worth 16x16 words: Transformers for image recognition at scale. *arXiv preprint arXiv:2010.11929*, 2020. 5

[4] Emilien Dupont, Hyunjik Kim, SM Ali Eslami, Danilo Jimenez Rezende, and Dan Rosenbaum. From data to functa: Your data point is a function and you can treat it like one. In *International Conference on Machine Learning*, pages 5694–5725. PMLR, 2022. 1

[5] Chelsea Finn, Pieter Abbeel, and Sergey Levine. Model-agnostic meta-learning for fast adaptation of deep networks. In *International conference on machine learning*, pages 1126–1135. PMLR, 2017. 3, 5

[6] Zekun Hao, Hadar Averbuch-Elor, Noah Snavely, and Serge Belongie. Dualsdf: Semantic shape manipulation using a two-level representation. In *Proceedings of the IEEE/CVF Conference on Computer Vision and Pattern Recognition*, pages 7631–7641, 2020. 2

[7] Jianwen Lou, Xiaoxu Cai, Junyu Dong, and Hui Yu. Real-time 3d facial tracking via cascaded compositional learning. *IEEE Transactions on Image Processing*, 30:3844–3857, 2021. 2

[8] Jianwen Lou, Yiming Wang, Charles Nduka, Mahyar Hamedi, Ifigeneia Mavridou, Fei-Yue Wang, and Hui Yu. Realistic facial expression reconstruction for vr hmd users. *IEEE Transactions on Multimedia*, 22(3):730–743, 2019. 2

[9] Julien NP Martel, David B Lindell, Connor Z Lin, Eric R Chan, Marco Monteiro, and Gordon Wetzstein. Acorn: Adaptive coordinate networks for neural scene representation. *arXiv preprint arXiv:2105.02788*, 2021. 1, 2, 14

[10] Daniel Meister, Shinji Ogaki, Carsten Benthin, Michael J Doyle, Michael Guthe, and Jiří Bittner. A survey on bounding volume hierarchies for ray tracing. In *Computer Graphics Forum*, volume 40, pages 683–712, 2021. 2

[11] Mateusz Michalkiewicz, Jhony K Pontes, Dominic Jack, Mahsa Baktashmotlagh, and Anders Eriksson. Implicit surface representations as layers in neural networks. In *Proceedings of the IEEE/CVF International Conference on Computer Vision*, pages 4743–4752, 2019. 2

[12] Ben Mildenhall, Pratul P Srinivasan, Matthew Tancik, Jonathan T Barron, Ravi Ramamoorthi, and Ren Ng. Nerf: Representing scenes as neural radiance fields for view synthesis. *Communications of the ACM*, 65(1):99–106, 2021. 1, 2, 16

[13] Alex Nichol, Joshua Achiam, and John Schulman. On first-order meta-learning algorithms. *arXiv preprint arXiv:1803.02999*, 2018. 3

[14] Michael Niemeyer and Andreas Geiger. Giraffe: Representing scenes as compositional generative neural feature fields. In *Proceedings of IEEE/CVF Conference on Computer Vision and Pattern Recognition*, pages 11453–11464, 2021. 2

[15] Henri J Nussbaumer. The fast fourier transform. In *Fast Fourier Transform and Convolution Algorithms*, pages 80–111. Springer, 1981. 12

[16] Jeong Joon Park, Peter Florence, Julian Straub, Richard Newcombe, and Steven Lovegrove. Deepsdf: Learning continuous signed distance functions for shape representation. In *Proceedings of the IEEE/CVF conference on computer vision and pattern recognition*, pages 165–174, 2019. 2

[17] Samuel Pfrommer, Mathew Halm, and Michael Posa. Contactnets: Learning discontinuous contact dynamics with smooth, implicit representations. *arXiv preprint arXiv:2009.11193*, 2020. 2

[18] Dian Qin, Haishuai Wang, Zhe Liu, Hongjia Xu, Sheng Zhou, and Jiajun Bu. Hilbert distillation for cross-dimensionality networks. *Advances in Neural Information Processing Systems*, 35:11726–11738, 2022. 2

[19] Nasim Rahaman, Aristide Baratin, Devansh Arpit, Felix Draxler, Min Lin, Fred Hamprecht, Yoshua Bengio, and Aaron Courville. On the spectral bias of neural networks. In *International Conference on Machine Learning*, pages 5301–5310. PMLR, 2019. 1, 2, 4, 8

[20] Maziar Raissi, Paris Perdikaris, and George E Karniadakis. Physics-informed neural networks: A deep learning framework for solving forward and inverse problems involving nonlinear partial differential equations. *Journal of Computational physics*, 378:686–707, 2019. 2

[21] Daniel Rebain, Wei Jiang, Soroosh Yazdani, Ke Li, Kwang Moo Yi, and Andrea Tagliasacchi. Derf: Decomposed radiance fields. In *Proceedings of the IEEE/CVF Conference on Computer Vision and Pattern Recognition*, pages 14153–14161, 2021. 2, 5

[22] Christian Reiser, Songyou Peng, Yiyi Liao, and Andreas Geiger. Kilonerf: Speeding up neural radiance fields with thousands of tiny mlps. In *IEEE/CVF International Conference on Computer Vision*, pages 14335–14345, 2021. 2, 5

[23] Peiran Ren, Jiaping Wang, Minmin Gong, Stephen Lin, Xin Tong, and Baining Guo. Global illumination with radiance regression functions. *ACM Trans. Graph.*, 32(4):130–1, 2013. 2

[24] Basri Ronen, David Jacobs, Yoni Kasten, and Shira Kritchman. The convergence rate of neural networks for learned functions of different frequencies. *Advances in Neural Information Processing Systems*, 32, 2019. 2

[25] Shunsuke Saito, Zeng Huang, Ryota Natsume, Shigeo Morishima, Angjoo Kanazawa, and Hao Li. Pifu: Pixel-aligned implicit function for high-resolution clothed human digitization. In *Proceedings of the IEEE/CVF International Conference on Computer Vision*, pages 2304–2314, 2019. 2

[26] Shunsuke Saito, Jinlong Yang, Qianli Ma, and Michael J Black. Scanimate: Weakly supervised learning of skinned clothed avatar networks. In *Proceedings of the IEEE/CVF Conference on Computer Vision and Pattern Recognition*, pages 2886–2897, 2021. 2

[27] Katja Schwarz, Yiyi Liao, Michael Niemeyer, and Andreas Geiger. Graf: Generative radiance fields for 3d-aware image synthesis. *Advances in Neural Information Processing Systems*, 33:20154–20166, 2020. 2

[28] Vincent Sitzmann, Eric Chan, Richard Tucker, Noah Snavely, and Gordon Wetzstein. Metasdf: Meta-learning signed distance functions. *Advances in Neural Information Processing Systems*, 33:10136–10147, 2020. 2, 3, 4, 6, 7

[29] Vincent Sitzmann, Julien Martel, Alexander Bergman, David Lindell, and Gordon Wetzstein. Implicit neural representations with periodic activation functions. *Advances in Neural Information Processing Systems*, 33:7462–7473, 2020. 1, 2, 3, 6, 7, 12, 16

[30] Vincent Sitzmann, Michael Zollhöfer, and Gordon Wetzstein. Scene representation networks: Continuous 3d-structure-aware neural scene representations. *Advances in Neural Information Processing Systems*, 32, 2019. 2

[31] Ivan Skorokhodov, Savva Ignatyev, and Mohamed Elhoseiny. Adversarial generation of continuous images. In *Proceedings of the IEEE/CVF Conference on Computer Vision and Pattern Recognition*, pages 10753–10764, 2021. 1, 2

[32] Matthew Tancik, Vincent Casser, Xinchen Yan, Sabeek Pradhan, Ben Mildenhall, Pratul P Srinivasan, Jonathan T Barron, and Henrik Kretzschmar. Block-nerf: Scalable large scene neural view synthesis. In *Proceedings of the IEEE/CVF Conference on Computer Vision and Pattern Recognition*, pages 8248–8258, 2022. 2

[33] Matthew Tancik, Ben Mildenhall, Terrance Wang, Divi Schmidt, Pratul P Srinivasan, Jonathan T Barron, and Ren Ng. Learned initializations for optimizing coordinate-based neural representations. In *Proceedings of the IEEE/CVF Conference on Computer Vision and Pattern Recognition*, pages 2846–2855, 2021. 2, 3, 4, 7

[34] Matthew Tancik, Pratul Srinivasan, Ben Mildenhall, Sara Fridovich-Keil, Nithin Raghavan, Utkarsh Singhal, Ravi Ramamoorthi, Jonathan Barron, and Ren Ng. Fourier features let networks learn high frequency functions in low dimensional domains. *Advances in Neural Information Processing Systems*, 33:7537–7547, 2020. 1, 2, 4, 8

[35] Edgar Tretschk, Ayush Tewari, Vladislav Golyanik, Michael Zollhöfer, Carsten Stoll, and Christian Theobalt. Patchnets: Patch-based generalizable deep implicit 3d shape representations. In *European Conference on Computer Vision*, pages 293–309. Springer, 2020. 2

[36] Haithem Turki, Deva Ramanan, and Mahadev Satyanarayanan. Mega-nerf: Scalable construction of large-scale nerfs for virtual fly-throughs. In *Proceedings of the IEEE/CVF Conference on Computer Vision and Pattern Recognition*, pages 12922–12931, 2022. 2

[37] Peihao Wang, Zhiwen Fan, Tianlong Chen, and Zhangyang Wang. Neural implicit dictionary learning via mixture-of-expert training. In *International Conference on Machine Learning*, pages 22613–22624. PMLR, 2022. 2

[38] Zhou Wang, Alan C Bovik, Hamid R Sheikh, and Eero P Simoncelli. Image quality assessment: from error visibility to structural similarity. *IEEE transactions on image processing*, 13(4):600–612, 2004. 17

[39] Yiheng Xie, Towaki Takikawa, Shunsuke Saito, Or Litany, Shiqin Yan, Numair Khan, Federico Tombari, James Tompkin, Vincent Sitzmann, and Srinath Sridhar. Neural fields in visual computing and beyond. In *Computer Graphics Forum*, volume 41, pages 641–676. Wiley Online Library, 2022. 2

[40] Zhi-Qin John Xu, Yaoyu Zhang, and Tao Luo. Overview frequency principle/spectral bias in deep learning. *arXiv preprint arXiv:2201.07395*, 2022. 2

[41] Zhi-Qin John Xu, Yaoyu Zhang, Tao Luo, Yanyang Xiao, and Zheng Ma. Frequency principle: Fourier analysis sheds light on deep neural networks. *arXiv preprint arXiv:1901.06523*, 2019. 2

[42] Tarun Yenamandra, Ayush Tewari, Florian Bernard, Hans-Peter Seidel, Mohamed Elgharib, Daniel Cremers, and Christian Theobalt. i3dmm: Deep implicit 3d morphable model of human heads. In *Proceedings of the IEEE/CVF Conference on Computer Vision and Pattern Recognition*, pages 12803–12813, 2021. 2

[43] Fisher Yu, Yinda Zhang, Shuran Song, Ari Seff, and Jianxiong Xiao. Lsun: Construction of a large-scale image dataset using deep learning with humans in the loop. *arXiv preprint arXiv:1506.03365*, 2015. 7, 12

[44] Gizem Yüce, Guillermo Ortiz-Jiménez, Beril Besbinar, and Pascal Frossard. A structured dictionary perspective on implicit neural representations. In *Proceedings of the IEEE/CVF Conference on Computer Vision and Pattern Recognition*, pages 19228–19238, 2022. 2, 3, 4, 7, 8

[45] Richard Zhang, Phillip Isola, Alexei A Efros, Eli Shechtman, and Oliver Wang. The unreasonable effectiveness of deep features as a perceptual metric. In *Proceedings of the IEEE conference on computer vision and pattern recognition*, pages 586–595, 2018. 17

[46] Sheng Zhou, Yucheng Wang, Defang Chen, Jiawei Chen, Xin Wang, Can Wang, and Jiajun Bu. Distilling holistic knowledge with graph neural networks. In *Proceedings of the IEEE/CVF international conference on computer vision*, pages 10387–10396, 2021. 2